Nanoscale

Accepted Manuscript

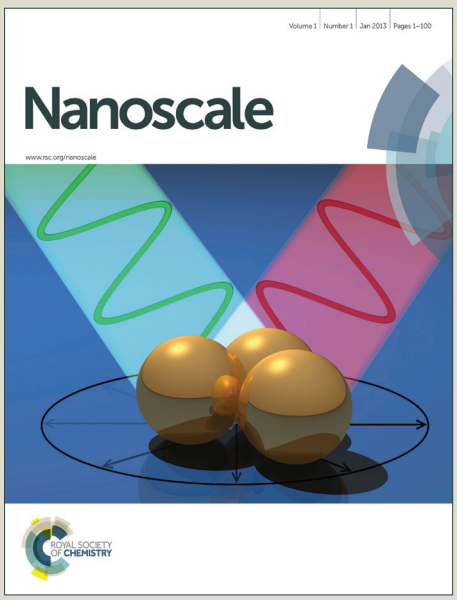

This is an *Accepted Manuscript*, which has been through the Royal Society of Chemistry peer review process and has been accepted for publication.

Accepted Manuscripts are published online shortly after acceptance, before technical editing, formatting and proof reading. Using this free service, authors can make their results available to the community, in citable form, before we publish the edited article. We will replace this *Accepted Manuscript* with the edited and formatted *Advance Article* as soon as it is available.

You can find more information about *Accepted Manuscripts* in the Information for Authors.

Please note that technical editing may introduce minor changes to the text and/or graphics, which may alter content. The journal's standard Terms & Conditions and the Ethical guidelines still apply. In no event shall the Royal Society of Chemistry be held responsible for any errors or omissions in this *Accepted Manuscript* or any consequences arising from the use of any information it contains.

ROYAL SOCIETY OF CHEMISTRY

www.rsc.org/nanoscale

Please do not adjust margins

Journal Name

ARTICLE

Ion-ion interactions in β-$NaGdF_4$:Yb^{3+}, Er^{3+} nanocrystals – effect of ions concentration and their clustering

Received 00th January 20xx,
Accepted 00th January 20xx

DOI: 10.1039/x0xx00000x

www.rsc.org/

A. Noculak,[a] A. Podhorodecki,*[a] G. Pawlik,[b] M. Banski[a] and J. Misiewicz[a]

In this work we report co-thermolysis as a proper method for the nanomaterials synthesis which allows to create hexagonal upconverting nanocrystals – $NaGdF_4$:Yb^{3+},Er^{3+} in wide range of sizes (20-120 nm). Only very high Yb^{3+} concentration (above 70%) results in pure cubic-phase nanocrystals with irregular shape. Additionally, we showed that impact of Yb^{3+}, Er^{3+} and Gd^{3+} ions on size and optical properties of nanocrystals is significant. We found that main changes in optical properties does not depend on nanocrystals size mostly, but are determined by the ion-ion interactions which include both Er^{3+}-Er^{3+} and Er^{3+}-Yb^{3+} cross relaxation.

Introduction

Colloidal nanocrystals (NCs) are of great fundamental and technical interest, due to their unique optical and magnetic properties and their potential applications in medicine. Especially, rare earth-doped fluoride nanocrystals (RENCs) are considered as promising tools for non-invasive *in vivo* and in *vitro* multimodal imaging of upconverted emission combined with X-ray computed tomography (CT)[1–3], magnetic resonance imaging (MRI)[4–8], single-photon emission computed tomography (SPECT) and positron emission tomography (PET) imaging[9–11].

Most of the lanthanide ions have to be excited in ultraviolet and blue spectral region. However, high energy photons cause optical photodamage of a biological tissue and give rise to undesirable autofluorescence signal from fluorophores placed in human body[12]. To overcome these obstacles an unique upconversion (UPC) process can be applied. In this process, visible emission are generated after the near-infrared **(**NIR) excitation of lanthanide-doped material. This NIR excitation with large anti-Stokes shift, sharp emission bandwidth, long fluorescence lifetime, tunable emission, and low-power excitation (comparing to two-photon absorption and SHG generation) constitute important advantages of this RENCs and allow for more straightforward signal detection[13]. Additionally, deep light penetration[14], suppressed autofluorescence, lack of photobleaching and photoblinking[15] and a low phototoxicity[16] make upconverting, fluoride RENCs suitable for *in vitro* and *in vivo* imaging[4,6,13].

Rare earth ions are generally characterized by low absorption cross-section (~10^{-21} cm^2), however some of them possess significantly higher absorption cross-section[17]. This is for example Yb^{3+} ($1.16 \cdot 10^{-20}$ cm^2) ion which, in addition, has very simple energy levels scheme[17]. Its $^2F_{7/2}$–$^2F_{5/2}$ transition is well resonant with f-f transitions of few lanthanide ions (Er^{3+}, Tm^{3+} and Ho^{3+}), that is why these elements constitute the most efficient upconverting activators. In cubic sodium rare earth fluoride systems ($NaREF_4$) fluorite structures (CaF_2) are formed and they contain one type of high-symmetry cation site randomly occupied by Na^+ and RE^{3+} ions. In hexagonal phase of $NaREF_4$ ordered array of F^- ions with two types of relatively low-symmetry cation sites selectively occupied by Na^+ and RE^{3+} ions, is present[18].

Despite using the most efficient upconverting activators, the efficient coupling between lanthanide ions become a key issue in order to obtain an intense emission. Additionally, when the crystal size is reduced to nanoscale, the UPC efficiency is reduced because of a presence of different surface quenching sites (surface defects, additional ions, ligands, and solvent molecules)[19,20]. Thus, the best UPC quantum yields emission ranges between 2 and 5% and is reduced significantly for RENCs belowe 10 nm [21,22]. This small quantum efficiency can be an effect of nonhomogeneous distribution of lanthanide ions or not optimal relative concentration of them and in consequence creation of Er^{3+} and Yb^{3+} clusters responsible for emission quenching, i.e. via the energy migration to the surface[23]. Moreover, there is no discussion in literature from which sizes of nanocrystals, the surface effects become significant and visible in optical measurements. For these nanoparticles shell protection indeed should significantly increase emission intensity.

Most of the reported results are obtained for RENCs with the size between 20 and 50 nm[24–27] and only few groups synthesized UPC RENCs with the size smaller than 15 nm[28–30].

[a] Department of Experimental Physics, Wroclaw University of Technology, Wyb. Wyspianskiego 27, 50-370 Wroclaw, Poland
[b] Department of Theoretical Physics, Wroclaw University of Technology, Wyb. Wyspianskiego 27, 50-370 Wroclaw, Poland

† Footnotes relating to the title and/or authors should appear here. Electronic Supplementary Information (ESI) available: [details of any supplementary information available should be included here]. See DOI: 10.1039/x0xx00000x

Nanoscale Accepted Manuscript

Please do not adjust margins

Small size in biomedical applications is required because of the possibility of using a higher dose of imaging agents and controlled body clearance [31]. Thus, despite recent progress in a synthesis of sub-15 nm and monodisperse RENCs an efficient near-infrared to visible (NIR-to-Vis) energy transfer and intense emission still remain major challenges. This is because, the size of the RENCs and the intensity of UPC emission are, in general, dependent parameters. Therefore, it is important to understand the mechanisms of ion-ion interactions in different-size RENCs to keep good optical properties regardless of their size. It is also important to investigate the ion-ion coupling efficiency, what can be done by detailed analysis of NIR spectra range. Such kind of results are not widely reported so far.

Another important challenge in this research is to control the size of RENCs in a wide range, keeping the narrow size distribution and β-phase, which is suitable for high quality optical markers. These features can be controlled using various synthesis parameters: temperature[32], ligand to solvent ratio[30], alkaline earth metals doping[33]. Moreover, different concentrations of lanthanide ions can result in various morphology and size of obtained RENCs[34].

It has been shown that Gd^{3+} ions can alert the fundamental nucleation and growth process of $NaYF_4$ RENCs during hydrothermal synthesis, what results in tuning their size[35]. Similar results were obtained by Li et al.[27] who synthesized various kinds of fluoride RENCs using co-thermolysis method and confirmed that the formation of monodisperse RENCs closely correlates with the inherent nature of lanthanide series from lanthanum (La^{3+}) to lutetium (Lu^{3+}). Smaller ionic radius of dopant gave result in formation of bigger RENCs. Effect of doping was theoretically explained by Wang et al.[18] who used first-principles calculations to confirm that influence of lanthanide doping on crystal phase and size arises from strong dependence on the size and dipole polarizability of the substitution dopant ion. Recently Damasco et al.[26] have shown that introduction of Gd^{3+} ions to the $NaYbF_4$ matrix can induce a significant decrease in the size of the nanoparticles. Low concentration of Gd^{3+} ions in crystal matrix caused formation of big (above 100 nm) RENCs, while high concentration allowed to obtain small RENCs. Such phenomena was ascribed to the changes of the surface charge density. Larger radius of Gd^{3+} ions (r = 93.5 pm) leads to a less electropositive surface in comparison with the smaller Yb^{3+} ions (r = 86.8 pm)[26,36]. This decreases a diffusion rate of the F^- ions to the surface of RENCs and thus limits a particle growth. Because of the correlation between RENCs size and dopants concentration it is difficult to judge which of these factors has a dominant influence on the optical properties.

Herein, we present the results of $NaGdF_4$:Yb^{3+},Er^{3+} RENCs synthesis with various concentration of dopant ions. Strong correlation between the concentration of dopants (Yb^{3+}, Er^{3+} and Gd^{3+} ions) and size of obtained RENCs is observed. The UPC photoluminescence (PL) intensities and lifetimes of the resulting RENCs were studied and analysed in relation to their size and ions concentration. Based on optical spectroscopy and numerical simulation the ion-ion interactions have been discussed.

Experimental details

Synthesis of core nanocrystals

The applied synthetic method of β-$NaGdF_4$:Yb^{3+}, Er^{3+} RENCs was similar to the single step co-thermolysis method presented in our previous paper[37]. Sodium trifluoroacetate $Na(CF_3COO)$ (98%), ytterbium(III) trifluoroacetate hydrate $Yb(CF_3COO)_3$ x $3H_2O$ (99 %), gadolinium oxide Gd_2O_3, erbium oxide Er_2O_3, trifluoroacetic acid CF_3COOH, 1-octadecen ODE and oleic acid OA were purchased from Sigma Aldrich and used as received without further purification. Gd_2O_3 and Er_2O_3 were dissolved in trifluoroacetic acid. Appropriate amounts of precursors: 1.0 mmol of $Na(CF_3COO)$, and 0.4 mmol of lanthanides ($Gd(CF_3COO)_3$, $Yb(CF_3COO)_3$ and $Er(NO_3)_3$) were prepared in three necked flask.

For RENCs synthesis, the precursor mixture of appropriate lanthanides composition was added to 5 ml of OA and 5 ml of ODE and was degassed at 120°C while being stirred. After 60 min the reaction was purged with N_2 and the temperature was increased to 300°C. After 60 min the reaction was cooled to 70°C and excess acetone was added to precipitate the nanoparticles. The resulting material was collected by centrifugation and excess OA and ODE was removed by washing with acetone several times and finally redispersed in 4 ml of cyclohexane.

Synthesis of core/shell nanocrystals

0.25 mmol of $Na(CF_3COO)$ (98%), 0.1 mmol of gadolinium trifluoroacetate $Gd(CF_3COO)_3$ (98%) and 1 ml of previously synthesized core RENCs was added to 5 ml of OA and 5 ml of ODE and was degassed at 120°C while being stirred. After 60 min the reaction was purged with N_2 and the temperature was increased to 300°C. After 60 min the reaction was cooled to 70°C and excess acetone was added to precipitate the nanoparticles. The resulting core/shell RENCs were collected by centrifugation and excess OA and ODE was removed by washing with acetone several times and finally redispersed in 1 ml of cyclohexane.

Structural and optical characterisation

Samples for the TEM experiments were prepared by evaporating a dilute cyclohexane solution of the nanoparticles onto carbon coated copper grids and a FEI Tecnai G2 20 X-TWIN microscope equipped with an energy-dispersive X-ray microanalyser was used to obtain the TEM images and EDXS spectra of the nanoparticles. X-ray powder diffraction patterns were obtained using a Philips diffractometer supported by a parallel beam optic and CuKα1 radiation source, λ=0.15406 nm.

Nanoscale Accepted Manuscript

This journal is © The Royal Society of Chemistry 20xx

Optical measurements

For steady state PL as an excitation source, a 980-nm laser (Shanghai Dream Lasers technology SDL-980-LM-1000T) was used. A HR4000 spectrometer (Ocean Optics, Dunedin, FL, USA) and InGaAs linear CCD detector (Symphony® I line, Horiba Jobin-Yvon) were used as detection systems for measurements in the Vis and NIR spectral range, respectively. The PL decays were measured using pulsed laser (Opolette™, Opotek Inc., Carlsbad, CA, USA) coupled to a gated detection system.

Results and discussion

Structural results

In order to check the effect of dopant concentration on size and morphology of RENCs, we prepared two sets of samples: first set with Er^{3+} concentration equal to 5% and Yb^{3+} concentration ranging from 10 to 70% and second set with constant Yb^{3+} concentration (20%) and Er^{3+} concentration ranging from 1 to 70%. Also two samples: $NaErF_4$ and $NaYbF_4$ were prepared (as the references).

All synthesized RENCs show well-defined peaks in diffraction patterns, confirming their good crystallinity. The positions of diffraction peaks of RENCs were consistent with reference patterns of hexagonal (ICDD no: 27-0699) or cubic (ICDD no: 27-0697) $NaGdF_4$ crystals (Fig. 1(a), 1S). Hexagonal crystalline structures were determined for almost all synthesized RENCs. The only exception was observed for sample with exceptional high Yb^{3+} concentration (above 70%), where mixture of cubic and hexagonal phase was determined. Similar results were obtained by Wang et al. [18] and Damasco et al. [26]. Smaller radius of heavy lanthanides causes that they are less polarizable and less favourable for electron cloud distortion. Doping of heavier lanthanides into the host lattice can therefore result in preventing the α→β phase transition [26].

The additional proof of hexagonal phase formation is high resolution TEM (HRTEM) image presented in Fig. 1(b) showing the lattice distance of 0.532 nm, corresponding to d spacing for the {100} lattice plane in the hexagonal $NaGdF_4$ structure.

For low Yb^{3+} ions concentration in $NaGdF_4$ matrix small (~20 nm) RENCs were obtained and with increasing Yb^{3+} ions concentration the formation of a bigger crystals is observed (Fig. 2(a-b), 2S). Significant growth of RENCs diameter is observed for the Yb^{3+} ions concentration above 20% and above 50% stabilization of RENCs size takes place (Fig. 3(h)).

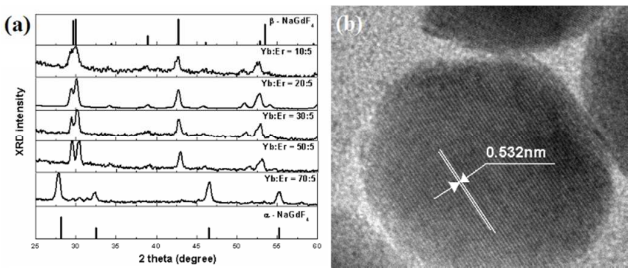

Fig. 1 XRD results (a) and lattice fringes (b) of $NaGdF_4$:Yb^{3+}, Er^{3+} RENCs with different Yb^{3+} ions concentration

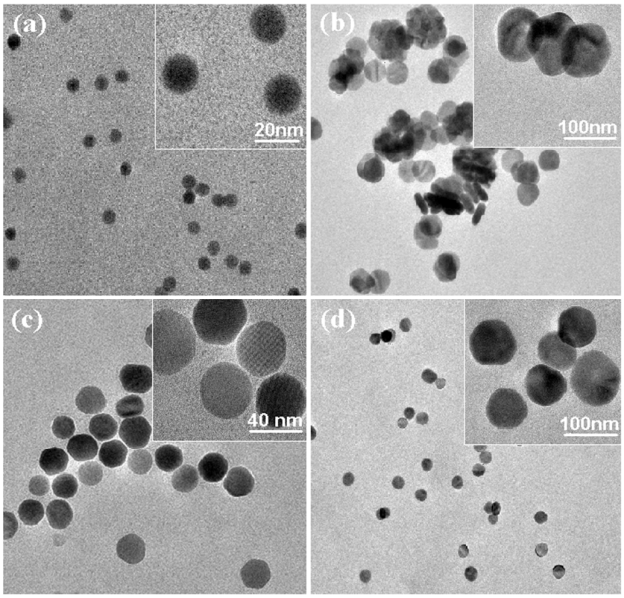

Fig. 2 TEM images of $NaGdF_4$:Yb^{3+}(10%),Er^{3+}(5%) (a), $NaGdF_4$:Yb^{3+}(40%),Er^{3+}(5%) (b), $NaGdF_4$:Yb^{3+}(20%),Er^{3+}(50%) (c) and $NaGdF_4$:Yb^{3+}(20%),Er^{3+}(70%) (d) RENCs

Additionally, for higher Yb^{3+} concentration (70 %) two distributions of RENCs sizes are observed (20 and 120 nm), what may indicate crystallization of RENCs in two different crystal phases (Fig. 2S). Higher increment of Yb^{3+} ions concentration till 100% ($NaYbF_4$) resulted in small (~20 nm) RENCs in pure α-phase.

Similar effect of dopant on size and phase of RENCs we observed for increasing concentration of Er^{3+} (Fig. 2(c-d), 3S). In this case strong influence of Er^{3+} ions on RENCs size is visible above 50% of Er^{3+} concentration, while below this value a size of RENCs is almost unchanged (Fig. 3(d)).

Change of the dopant concentration affects on RENCs surface charge, what may result in an increased or decreased diffusion rate of negatively charged F^- ions to the surface. This thesis based on density functional theory calculations and was proposed by Wang [18] and it refers to different ionic size of dopants. High concentration of Yb^{3+} and Er^{3+} ions in crystal matrix caused formation of big (above 100 nm) RENCs (except pure $NaYbF_4$ RENCs), while the low concentration allowed to obtain small RENCs. Because the ionic radius of Er^{3+} (89.0 pm) is closer to ionic radius of Gd^{3+} (93.5 pm) than Yb^{3+} (86.8 pm), changes in size of RENCs start to be visible for higher concentrations of Er^{3+} ions (above 50%) (Fig. 3(d)) while for Yb^{3+} ions are already present above 20% (Fig. 3(h)).

Moreover, the shape of big RENCs (with high Yb^{3+} or Er^{3+} concentrations) is more like hexagonal flakes (Fig. 2S, 3S). These $NaGdF_4$ RENCs show a preferred growth direction along [0001] and are enclosed by {10-10} and {0001} facets. Therefore, it can be concluded that the growth rate on the six lateral faces of the RENCs is faster than that along [0001] direction with increasing the RENCs size.

Nanoscale Accepted Manuscript

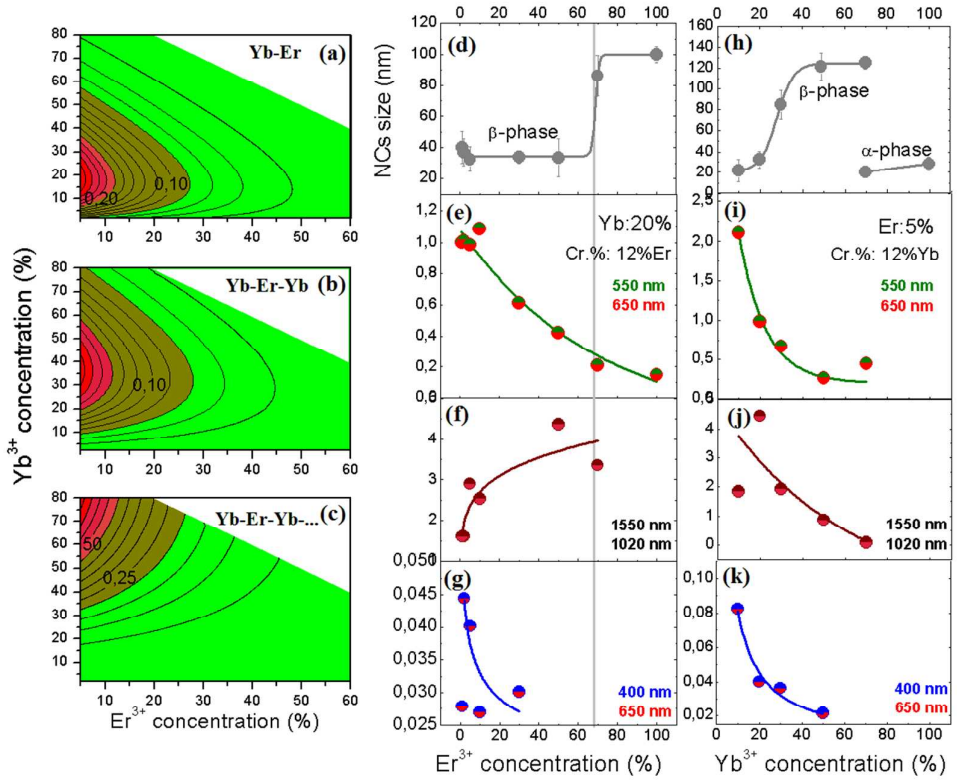

Fig. 3 Maps of probability of occurrence Yb^{3+}-Er^{3+} (a), Yb^{3+}-Er^{3+}-Yb^{3+} (Er^{3+}-Yb^{3+}-Er^{3+}) (b) and Yb^{3+}-Er^{3+}-Yb^{3+}-...Er^{3+} (c) interactions for different Yb^{3+} and Er^{3+} concentrations. Average RENCs sizes calculated from HRTEM for β-$NaGdF_4$: (20%)Yb^{3+}, Er^{3+} (d), and β-$NaGdF_4$: Yb^{3+}, (5%)Er^{3+} RENCs (h). Calculated ratio of different emission bands: G/R (e,i), NIR – Er, NIR-Yb (f,j), B/R (g,k)

Summarizing, in case of our RENCs the dopant concentration affects weakly on phase of RENCs. Only for very high Yb^{3+} concentration RENCs remained in α-phase (α→β phase transition did not occur). On the other hand, impact of Yb^{3+} ions concentration on size of RENCs is strongly prominent in entire range of Yb^{3+} concentration, while for Er^{3+} ions is visible above 50% of Er^{3+} ions concentration.

Optical results

In fluoride RENCs, the lanthanide ions take at least two significantly different positions: as surface ions (RE_S) or volume ions (RE_V) [34]. We have already shown, that for β-$NaYF_4$:Eu^{3+} RENCs, the excitation, emission and even the relaxation mechanisms for the surface and volume sites are different. This is due to differences in local environment (strength and symmetry of the local crystal field, local vibronic properties or surface chemistry) [34].

The phonon energies available for electrons in the excited states of Er^{3+} ions located inside the core (320 cm^{-1}) [38] are smaller than in case of ions placed at the RENCs surface. This is mainly because of the lower coordination number of atoms at the RENCs surface and presence of ligands (i.e. OH ≈ 3 700 cm^{-1} or CH_3 ≈ 3 000 cm^{-1}) in close vicinity of the ions. In consequence, depopulation of higher energy levels of Er^{3+} ions ($^2H_{11/2}$, $^4S_{3/2}$), responsible for the green emission should be less probable in case of RE_V (energy difference between $^4S_{3/2}$ and $^4F_{9/2}$ state is 3035 cm^{-1}, which corresponds to ~ 9 phonons) thus green light due to ($^2H_{11/2}$+$^4S_{3/2}$) → $^4I_{15/2}$ transitions should dominate the spectrum. In contrast, excited RE_S ions can efficiently relax non-radiativelly to "red emitting" ($^4F_{9/2}$) state, because only 1-2 high energy phonons are required to depopulate $^2H_{11/2}$ and $^4S_{3/2}$ states. Thus, dominating emission band should be the red one. Moreover, in this case the ions easily relax non-radiatively further from $^4F_{9/2}$ down to $^4I_{13/2}$ level increasing the emission at 1550 nm. In consequence, the emission from RE_S is spectrally more diffused, what makes emission intensities from individual states lower. Thus, the ratios of green-to-red (G/R) and green-to-NIR (G/NIR) emission intensity are lower for surface ions as compared to volume ions. Assuming homogeneous dopants distribution within entire RENC and from the fact that carriers relaxation depends on ions position (surface or volume) these ratios should depends on RENCs size as well. When the surface-to-volume ratio decreases the number of surface and volume ions is changed. Thus, in any case of macroscopic measurements we have always a superposition of signals coming from the ions placed at two sites: RE_S and RE_V. For the smallest RENCs, the dominating emission should be the red one ($^4F_{9/2}$ → $^4I_{15/2}$), because the number of RE_S is high in comparison to number of RE_V. Contrary, the big RENCs emission should be dominated by green emission (($^2H_{11/2}$+$^4S_{3/2}$) → $^4I_{15/2}$) coming from the RE_V. Thus, we should observe an increase in G/R ratio when changing RENCs size from small to big.

Nanoscale Accepted Manuscript

This journal is © The Royal Society of Chemistry 20xx

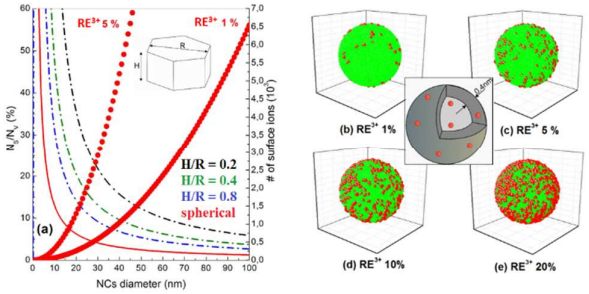

Fig. 4 Surface-to-volume ions ratio for different sizes and shapes of RENCs and number of surface ions for RENCs with different Er^{3+} concentration (a), process of clusters formation for different Yb^{3+} concentrations (b-e)

To get more intuition how the size of RENCs affects the optical properties, the numerical Monte Carlo simulations have been performed. First of all, Fig. 4(a) shows how the ratio between the number of surface and volume ions (N_S/N_V) is changing when the RENCs size is varied for 2 different shapes. We can see that the significant changes of N_S/N_V and thus changes of the relative emission intensities from RE_S and RE_V sites should be mainly visible for RENCs with the sizes around 20-30 nm. For our samples, the size of RENCs varies between 20-120 nm thus, we should not observe a significant influence of RENCs size on their optical properties.

In order to check experimentally if there is an influence of the RENCs surface on G/R ratio in case of our RENCs, we covered their surface with undoped $NaGdF_4$ thin (2.8 nm) shell layer. TEM images have been presented in Fig. 4S (a,b). After shell deposition G/R ratio slightly increased in comparison to core RENCs (Fig. 4S(c)). This means that for RENCs with sizes larger than 20 nm the surface effect is still visible, but is not very significant and weakly visible in optical measurements.

Figure 4 (b-e) presents simulated distributions of surface ions for 10 nm RENCs doped with a different ions concentrations. From these results we can see, how the variations in concentration of lanthanides influence on ions clusters formation, which causes efficient ion-ion interactions. These interactions, dependent on cluster character, can be responsible for an efficient depopulation of the *green emitting states* ($^2H_{11/2}$, $^4S_{3/2}$) down to *red emitting states* ($^4F_{9/2}$) of Er^{3+} ions in cross-relaxation (CR) process changing the observed G/R ratio. For example, for 10-15 nm hexagonal $NaYF_4$:Eu^{3+} RENCs we have estimated recently [34] that the significant increase in the ion-ion interactions (i.e. CR and energy migration) appears when Eu^{3+} ions concentration equals to 5% what corresponds to distance between the Eu^{3+} ions around 6.5 Å. This value is close to lattice constant of hexagonal phase of $NaYF_4$ (a=5.96 Å, b=3.53 Å) [18] suggesting that these interactions appear when two ions are very close each other, forming so-called *chemical clusters*. From Fig. 4(c) we can see that the clustering in case of Er^{3+} and Yb^{3+} co-doped $NaGdF_4$ RENCs should also appear at very low concentrations (around 5%).

Based on our numerical modelling, for whole 10 nm RENCs volume, we calculated also the probability of finding RE_1^{3+} - RE_2^{3+}, RE_1^{3+} - RE_2^{3+}- RE_1^{3+}, RE_1^{3+} - RE_2^{3+} -…- RE_1^{3+} clusters as a function of lanthanides concentration. Obtained results have been shown in Fig. 3(a, b, c). From Fig. 3(a) we can see that the highest probability of finding Er^{3+}-Yb^{3+} pairs is when the Er^{3+} concentration is below 10% and Yb^{3+} concentration is in the range from 10 to 25%. This simple lanthanides configuration enables Er^{3+} ions to be isolated from the other Er^{3+} ions and thus non-radiative relaxation like down-conversion (DC) or CR are suppressed. This range of Yb^{3+} concentration also limits the Yb^{3+}-Yb^{3+} energy migration (i.e. from volume to surface) and non-radiative recombination of absorbed photons. Thus, at this range of concentrations the green emission should dominate the spectrum. On the other hand, the excitation of Er^{3+} via Yb^{3+} ions cannot be optimal in this conditions, because only one Yb^{3+} take part in 2-step or 3-step excitation process of Er^{3+} ion (Fig. 5(a)).

From Fig. 3(b) we can see that for Er^{3+} concentrations below 10% and Yb^{3+} concentration above 25% the probability of finding Yb^{3+}-Er^{3+}-Yb^{3+} clusters increases. In this concentration range, the Er^{3+} ions can be excited by two or more Yb^{3+} ions via multiple 1-step process what makes this excitation path more probable. Thus, this range of concentration seems to be optimal for efficient and intense light emission from Er^{3+} ions, however the balance between efficiency of $Yb^{3+}\rightarrow Er^{3+}$ excitation, Yb^{3+}-Yb^{3+} interactions and emission from isolated Yb^{3+} ions should be found (Fig. 5(b,c)).

Higher Yb^{3+} concentration (above 50%) increases the probability of Yb^{3+} clusters formation (more than two Yb^{3+} ions as the first neighbours of Er^{3+} ions). This results in multiple unwanted events i.e. radiative emission of Yb^{3+} ions at 1020 nm, excitation energy migration to the surface, co-operative Yb^{3+} emission or back energy transfer (BET) from Er^{3+} to Yb^{3+} (Fig. 5 (c,d)). Thus, in this concentration range the emission is mainly red and the other processes like energy migration should be included what in consequence reduce also the total emission intensity from RENCs. The picture given above is symmetric and also can be discussed as Er^{3+}-Yb^{3+}-Er^{3+} and Er^{3+}-Yb^{3+}-Er^{3+}-…-Er^{3+} clusters formation which can promote the CR between Er^{3+} ions and increase surface losses of absorbed photons.

To validate our numerical predictions, regarding influence of Er^{3+} and Yb^{3+} concentrations on their interactions and optical properties of RENCs, we analysed a set of β-$NaGdF_4$:Yb^{3+}, Er^{3+} samples with different Yb^{3+} and Er^{3+} concentrations and obtained results have been shown in Fig. 3(d-k). First of all, from Fig. 3(d) we can see, that increase in Er^{3+} concentration, even up to 50%, do not change RENCs size. However, above this value, the RENCs size increases from 20-30 nm up to 100 nm without change in crystal phase. On the other hand, from Fig. 3(e) we can see that with increase in Er^{3+} content above 10 % the green-to-red emission intensity ratio decreases. This is the opposite tendency as expected for the size effect discussed above, indicated that observed changes in spectral response of RENCs are rather a consequence of Er^{3+}-Er^{3+} interactions (i.e. CR) which enables depopulation of *green states* to *red states* as the alternative to low probable multiphonon relaxation process. The significance of Er^{3+}-Er^{3+} interactions in our samples have been also confirmed by

Nanoscale Accepted Manuscript

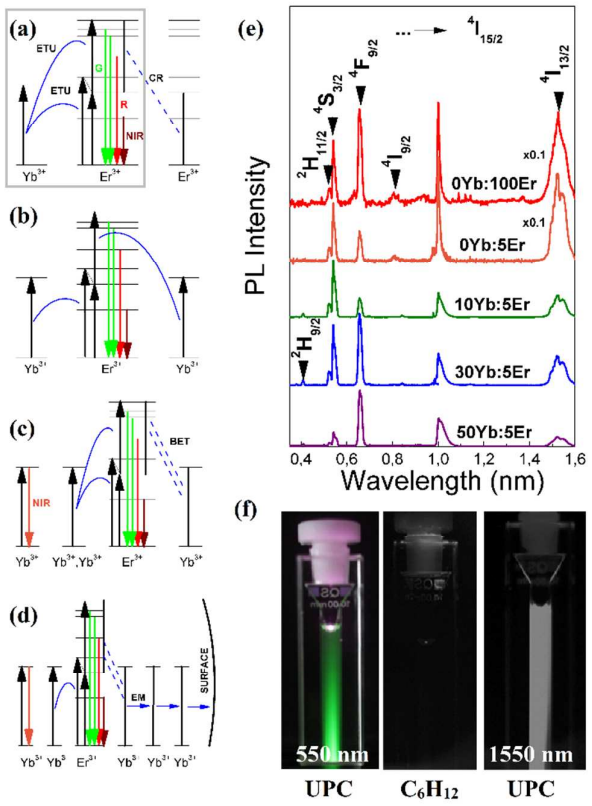

Fig. 5 Energy diagrams with radiative and non-radiative transitions for different Yb^{3+} ions concentration (a-d), normalized at 800 nm, but not corrected spectrally, emission spectra in VIS and NIR (e) and photo image of RENCs luminescence after 980 nm excitation – third photo was taken using 1100 nm edge filter (photo of the pure solvent has been added for comparison)

analysing the samples containing the Er^{3+} ions only. In this case, increase in number of Er^{3+} ions (from 5 to 100 %) decreases G/R ratio in the same way as for Yb^{3+}, Er^{3+} co-doped samples. Based on obtained results we can conclude, that for RENCs bigger than 20 nm the ion-ion interactions, not nanocrystal size, is the main factor influencing the optical properties of RENCs. Thus, our experimental results are in good agreement with numerical simulations.

From Fig. 3(f) we can see, that the ratio between the intensities of emission bands at 1550 and 1020 nm slightly increases with Er^{3+} concentration. Because concentration of Yb^{3+} ions is not increasing in this case, the changes in this ratio are due to Er^{3+} emission at 1550 nm or more effective energy transfer form Yb^{3+} to Er^{3+} ions (more Er^{3+} ions in close proximity of Yb^{3+} ions). At higher Er^{3+} concentration the relaxation from higher erbium levels is easier (Er^{3+}-Er^{3+} CR) down to $^4I_{13/2}$ level and in addition more Er^{3+} ions is excited directly to $^4I_{13/2}$ what results in increasing down shifting emission at 1550 nm. Meantime, emission from $^4S_{3/2}$ is suppressed. Figure 3(g) shows that also blue emission was still detectable for RENCs with Er^{3+} concentration below 20%. Above this value strong CR mechanisms reduce also the emission by relaxing carriers to the lower Er^{3+} states.

In Fig. 3(h) very similar tendency of RENCs sizes like in Fig. 3(d) has been observed when Yb^{3+} concentration increases. In this case however, increase in Yb^{3+} concentration influences the morphology of RENCs even at low concentrations of Yb^{3+} and increases their sizes from 20 to 120 nm. Nevertheless, despite these morphological differences, the tendency in G/R ratio is the same as for variations in Er^{3+} concentration.

Low concentration of Yb^{3+} causes that Er^{3+} ions can be excited via 2-step process, which is less efficient. When we increase the concentration of Yb^{3+} ions 2-step process can be replaced by 1-step multiple process and the excitation to higher energy levels is more probable. However, for higher Yb^{3+} concentration the energy migration among Yb^{3+} ions starts. Significant coupling between the Er^{3+} and Yb^{3+} ions and back energy transfer process which enables depopulation of ($^2H_{11/2}$+$^4S_{3/2}$) states down to $^4F_{9/2}$ states, increasing the contribution of red emission for highly Yb^{3+} doped RENCs. As a result emission from green states is decreased significantly while the emission from blue states is not. Nevertheless, the strongest emission is from the *red states*. In addition, from Fig. 3(j) we can see that with increase in Yb^{3+} concentration (except low Yb^{3+} concentration – 10 %, which causes that Yb^{3+} are Er^{3+} are separated from each other and the energy transfer is not efficient) we can observe a significant decrease in down-shifting Er^{3+} emission (1550 nm) and increase in Yb^{3+} emission (1020 nm). The reduction in this ratio is due to increase in Yb^{3+} emission. There is an optimal coupling between the Yb^{3+} and Er^{3+} ions and additional Yb^{3+} ions introduced into the matrix do not improve the UPC emission but only serve as 1020 nm emitters and reduce the green emission due to back energy transfer from Er^{3+} to Yb^{3+} ions. Also a higher Yb^{3+} content enabling existence of Yb^{3+}-Yb^{3+} networks where the excitation energy migration appears together with a non-radiative energy dissipation i.e. at the RENCs surface [39]. This process quench emission from our RENCs for Yb^{3+} concentration above 70%. All these conclusions are also consistent with our simulations results (Fig. 3(a-c)). Moreover, analyzing results shown in Fig. 3(k) we can see a significant reduction in blue to red ratio when Yb^{3+} concentration increases. This is also the consequence of depopulation of *blue states* via $Er^{3+}\rightarrow Yb^{3+}$ BET.

To analyse our results in more quantitative way, relative changes in emission bands in VIS and NIR spectral range have been analysed and shown in Fig. 5. The emission spectra were recorded in a wide spectral range from 200 to 1600 nm by two different CCD detectors. The Er^{3+} emission band at around 800 nm ($^4I_{9/2}$-$^4I_{15/2}$) was measured on both detectors and then was used to normalize the emission spectra recorded at two spectral ranges. This procedure enables us to analyse in quantitative way the changes in the ratio between the down shifting emission (1550 nm or 1020 nm) and up-converting emission between different samples. Firstly, from Fig. 5 we can see that when there is no Yb^{3+} in the RENCs ($NaGdF_4$:Er^{3+}) upconverting emission is still present in the samples due to self-absorption process, however, it is at least 10 times less intense than down shifting emission at 1550 nm.

Nanoscale Accepted Manuscript

This journal is © The Royal Society of Chemistry 20xx

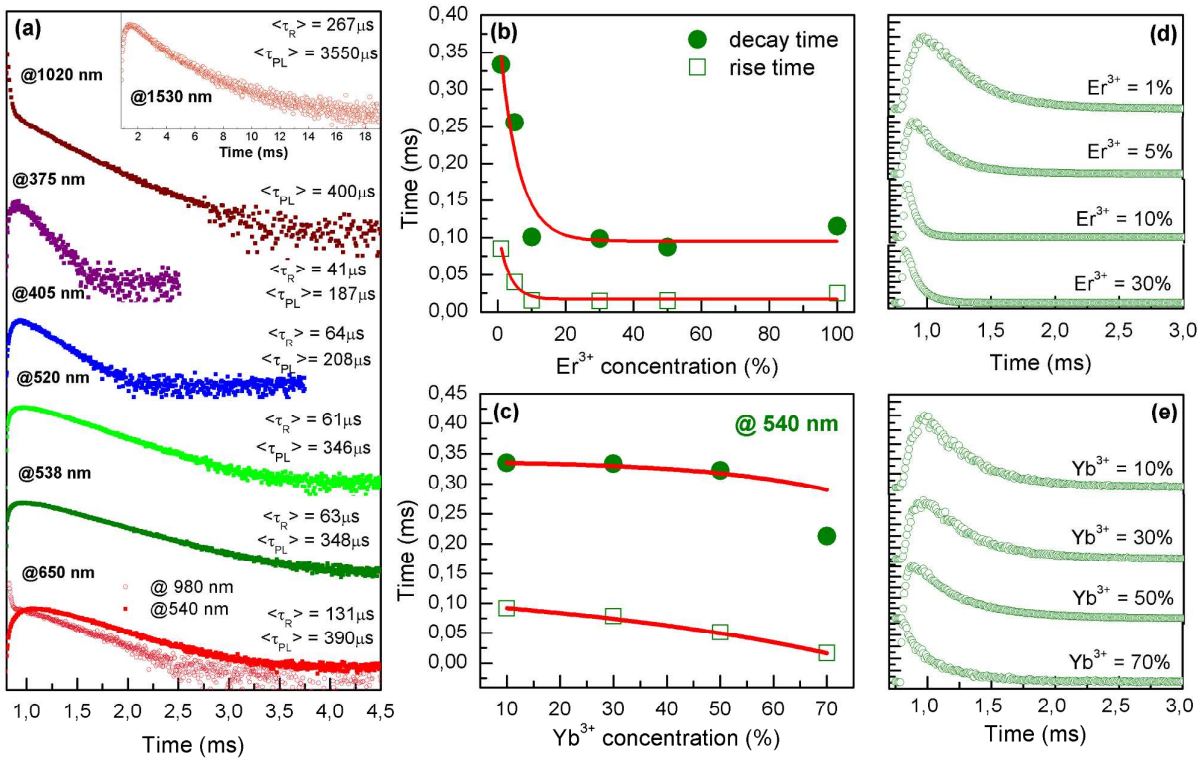

Fig. 6 Emission decay curves of β-$NaGdF_4$:Yb^{3+} (20%), Er^{3+} (2%) RENCs recorded at different emission wavelengths under 980 nm excitation (a). Average decay and rise times of emission at 540 nm of β-$NaGdF_4$:Yb^{3+}, Er^{3+} RENCs with different Er^{3+} (b) and Yb^{3+} (c) concentrations. Decay curves for different Er^{3+} (d) and Yb^{3+} (e) concentrations.

From green-to-red emission intensity for two samples with a different Er^{3+} concentrations (no Yb^{3+}) we can also see that increase in Er^{3+} concentration reduces the green-to-red emission intensity ratio. This tendency is similar for co-doped samples, like it was shown in Fig. 3(e). In addition, the green emission observed for $NaErF_4$ sample is significantly lower than in case of low doping regime (5% of Er^{3+}) due to ion-ion quenching effects i.e. excitation energy migration to surface and its non-radiative dissipation. Secondly, from Fig. 5 we can see, that adding to $NaGdF_4$:5%Er^{3+} RENCs 10% of Yb^{3+} does not change the (G/R) ratio significantly but the up-converting emission increasing around 10 times in relation to down-shifting emission at 1550 nm when compared to Yb^{3+} free samples. Thus, it is a clear evidence that Yb^{3+} ions participate in the efficient Er^{3+} excitation and improve UPC emission intensity even if some of the photons have been still lost in radiative Yb^{3+} emission or due to down-shifting Er^{3+} emission at 1550 nm. Also in case of all $NaGdF_4$: Yb^{3+}, Er^{3+} samples, we can see a week emission at around 400 nm which was absent in case of $NaGdF_4$:Er^{3+} samples due to weak efficiency of self-absorption process as compared to multi-step energy transfer from Yb^{3+} to Er^{3+} ions. Moreover, after detailed analysis of the emission spectra shown in Fig. 5 we did not found indication of Yb^{3+} co-operative emission, usually observed at 500 nm, and thus evidence of isolated Yb^{3+} chemical clustering.

In the next step, to better understand the Er^{3+}-Yb^{3+} and Er^{3+}-Er^{3+} interactions in our RENCs, the photoluminescence kinetics have been investigated. Since the model of interacting Er^{3+}-Yb^{3+} ions pair relaxation is complex and should be farther expanded in order to takes into account the variation of Er^{3+} and Yb^{3+} concentrations and different positions in lattice, we analysed our results qualitatively using an average decay time approach. Figure 6(a) shows the emission decay curves of the β-$NaGdF_4$:Yb^{3+} (20%), Er^{3+} (2%) sample detected at different emission bands, under 980 nm excitation. The decay time varies between 187 and 400 μs for visible emission bands and is significantly longer for 1550 nm band (3550 μs). For all emissions bands however, the emission rise time is similar (~65 μs) and the most probably relates to time needed to transfer the excitation energy from Yb^{3+} to Er^{3+} ions. To confirm this hypothesis, the Er^{3+} emission decay time of a red band at 650 nm has been measured at two excitation wavelength 980 nm and quasi-resonantly at 540 nm. Independent on the excitation wavelength the red emission band has the same decay time. However, the emission rise time is below the resolution of our setup (~2 μs) for quasi-resonant excitation. This result suggests, that the relaxation within the Er^{3+} ions is a fast process (<2 μs), while the energy transfer from Yb^{3+} to Er^{3+} ions is slow (order of dozens of μs). The long rise time suggests that the Yb^{3+}-Er^{3+} energy transfer is

Nanoscale Accepted Manuscript

dipole-dipole type interaction and energy migration UPC (EMU) can take also place[40].

More detailed analysis are summarized in Fig. 6 (b-c) where the decay times of a green emission at 540 nm have been shown for samples with different Yb^{3+} and Er^{3+} content. When the Er^{3+} ions concentration increases the emission decay time exponentially reduces. This is because the Er^{3+}-Er^{3+} coupling became more efficient and that ion-ion interaction influences the emission decay time via the non-radiative component (τ_{NRad}) of emission decay time

$$\frac{1}{\tau_{PL}} = \frac{1}{\tau_{Rad}} + \frac{1}{\tau_{NRad}}.$$

Similar reduction in rise time can be due to more probable coupling between Er^{3+} ions at higher Er^{3+} ions concentration.

The situation is very different however, when Yb^{3+} content in β-$NaGdF_4$:Yb^{3+}, Er^{3+}(5%) RENCs is changing. In this case, the green emission decay time is almost constant in the entire range of Yb^{3+} concentration. This is because the green emission of Er^{3+} ions is not in resonance with Yb^{3+} levels thus resonant dipole-dipole interactions reducing τ_{PL} can be excluded. However, for increasing Yb^{3+} concentration we observed decrease in the green emission rise time, which may be an effect of more efficient Yb^{3+} to Er^{3+} ET, because of the presence of higher numbers of sensitizers (Yb^{3+} ions).

Conclusions

In summary, we have investigated the impact of dopant concentration on phase, size and optical properties of Er^{3+} and Yb^{3+}-doped $NaGdF_4$ RENCs. It has been shown that hexagonal crystal phase of RENCs can be maintained for a wide range of dopants concentration. Only high Yb^{3+} concentration resulted in formation of RENCs in cubic phase, because of the raising of energy barrier for α→β phase transitions due to doping of the smaller ions. Physical properties of lanthanides, like ionic size, strongly influence the morphology of obtained RENCs, especially on size of RENCs. When extent of Er^{3+} and Yb^{3+} substitution of Gd^{3+} ions increases, the size of RENCs grows. Because ionic radius decreases in order Gd^{3+} (93.5 pm), Er^{3+} (89 pm) and Yb^{3+} (86.8 pm) the change in the size of RENCs is detectable at 60% of Er^{3+} concentration, while 20% of Yb^{3+} ions doping is enough to influence the size of RENCs.

Because, both dopants concentration and RENCs size influence optical properties of upconverting RENCs, and in our synthesis these are dependent parameters, the analysis of the impact of Er^{3+}, Yb^{3+} ions concentration on photoluminescence is challenging. However, according to our numerical simulations impact of RENCs size on their optical properties (eg. G/R emission ratio) is negligible for RENCs bigger than 20 nm. This was further confirmed through investigation of core-shell structures. We suggests, that in case of investigated RENCs, the intensities of particular emission bands are primarily governed by formation of dopants clusters and their efficient ion-ion interactions. Because of that, with increasing both Yb^{3+} and Er^{3+} the emission from green states is reduced, while the emission from red states is increased. Additionally, we showed, that at high Yb^{3+} concentration less desirable cubic phase is obtained. Such RENCs do not show an improved UPC emission but rather serve as efficient down-converting emitters at 1020 nm.

Acknowledgments

This work was supported by the grants from the National Science Centre, Sonata Bis 3 Project No. UMO-2013/10/E/ST5/00651. M.B would like to acknowledge Foundation for Polish Science (FNP) "Start" for the financial support. A.N would like to acknowledge Ministry of Science and Higher Education in Poland for the financial support.

1 J. Ma, P. Huang, M. He, L. Pan, Z. Zhou, L. Feng, G. Gao and D. Cui, *J. Phys. Chem. B*, 2012, **116**, 14062–14070.
2 J.-W. Shen, C.-X. Yang, L.-X. Dong, H.-R. Sun, K. Gao and X.-P. Yan, *Anal. Chem.*, 2013, **85**, 12166–12172.
3G. Zhang, Y. Liu, Q. Yuan, C. Zong, J. Liu and L. Lu, *Nanoscale*, 2011, **3**, 4365–4371.
4 G. Chen, H. Qiu, P. N. Prasad and X. Chen, *Chem. Rev.*, 2014, **114**, 5161–5214.
5 C. Liu, Z. Gao, J. Zeng, Y. Hou, F. Fang, Y. Li, R. Qiao, L. Shen, H. Lei, W. Yang and M. Gao, *ACS Nano*, 2013, **7**, 7227–7240.
6 Y. Min, J. Li, F. Liu, P. Padmanabhan, E. K. L. Yeow and B. Xing, *Nanomaterials*, 2014, **4**, 129–154.
7 D. Ni, J. Zhang, W. Bu, H. Xing, F. Han, Q. Xiao, Z. Yao, F. Chen, Q. He, J. Liu, S. Zhang, W. Fan, L. Zhou, W. Peng and J. Shi, *ACS Nano*, 2014, **8**, 1231–1242.
8 X. Zhu, J. Zhou, M. Chen, M. Shi, W. Feng and F. Li, *Biomaterials*, 2012, **33**, 4618–4627.
9 Q. Liu, Y. Sun, C. Li, J. Zhou, C. Li, T. Yang, X. Zhang, T. Yi, D. Wu and F. Li, *ACS Nano*, 2011, **5**, 3146–3157.
10J. Peng, Y. Sun, L. Zhao, Y. Wu, W. Feng, Y. Gao and F. Li, *Biomaterials*, 2013, **34**, 9535–9544.
11Y. Sun, X. Zhu, J. Peng and F. Li, *ACS Nano*, 2013, **7**, 11290–11300.
12C. T. Xu, N. Svensson, J. Axelsson, P. Svenmarker, G. Somesfalean, G. Chen, H. Liang, H. Liu, Z. Zhang and S. Andersson-Engels, *Appl. Phys. Lett.*, 2008, **93**, 171103.
13F. Wang, D. Banerjee, Y. Liu, X. Chen and X. Liu, *Analyst*, 2010, **135**, 1839–1854.
14H. Arimoto and M. Egawa, *Skin Res. Technol.*, 2014, n/a–n/a.
15Y. I. Park, K. T. Lee, Y. D. Suh and T. Hyeon, *Chem Soc Rev*, 2014.
16B. Sojka, M. Kuricova, A. Liskova, M. Bartusova, M. Banski, J. Misiewicz, M. Dusinska, M. Horvathova, E. Jahnova, S. Ilavska, M. Szabova, E. Rollerova, A. Podhorodecki and J. Tulinska, *J. Appl. Toxicol. JAT*, 2014, **34**, 1220–1225.
17V. A. Lebedev, V. F. Pisarenko, N. V. Selina, A. A. Perfilin and M. G. Brik, *Opt. Mater.*, 2000, **14**, 121–126.
18F. Wang, Y. Han, C. S. Lim, Y. Lu, J. Wang, J. Xu, H. Chen, C. Zhang, M. Hong and X. Liu, *Nature*, 2010, **463**, 1061–1065.
19Y. Sun, Y. Chen, L. Tian, Y. Yu, X. Kong, J. Zhao and H. Zhang, *Nanotechnology*, 2007, **18**, 275609.
20Q. Su, S. Han, X. Xie, H. Zhu, H. Chen, C.-K. Chen, R.-S. Liu, X. Chen, F. Wang and X. Liu, *J. Am. Chem. Soc.*, 2012, **134**, 20849–20857.
21N. C. Dyck, F. C. J. M. van Veggel and G. P. Demopoulos, *ACS Appl. Mater. Interfaces*, 2013, **5**, 11661–11667.

Nanoscale Accepted Manuscript

This journal is © The Royal Society of Chemistry 20xx

22S. Wilhelm, M. Kaiser, C. Würth, J. Heiland, C. Carrillo-Carrion, V. Muhr, O. S. Wolfbeis, W. J. Parak, U. Resch-Genger and T. Hirsch, *Nanoscale*, 2015, **7**, 1403–1410.
23J. Wang, R. Deng, M. A. MacDonald, B. Chen, J. Yuan, F. Wang, D. Chi, T. S. Andy Hor, P. Zhang, G. Liu, Y. Han and X. Liu, *Nat. Mater.*, 2014, **13**, 157–162.
24Q. Cheng, J. Sui and W. Cai, *Nanoscale*, 2012, **4**, 779–784.
25A. Noculak, Y. S. Fhui, M. Banski, J. Misiewicz and A. Podhorodecki, *J. Nanoparticle Res.*, 2014, **16**, 1–9.
26J. A. Damasco, G. Chen, W. Shao, H. Ågren, H. Huang, W. Song, J. F. Lovell and P. N. Prasad, *ACS Appl. Mater. Interfaces*, 2014, **6**, 13884–13893.
27X. Li, S. Gai, C. Li, D. Wang, N. Niu, F. He and P. Yang, *Inorg. Chem.*, 2012, **51**, 3963–3971.
28G. Chen, T. Y. Ohulchanskyy, R. Kumar, H. Ågren and P. N. Prasad, *ACS Nano*, 2010, **4**, 3163–3168.
29N. J. J. Johnson, W. Oakden, G. J. Stanisz, R. Scott Prosser and F. C. J. M. van Veggel, *Chem. Mater.*, 2011, **23**, 3714–3722.
30J. Ryu, H.-Y. Park, K. Kim, H. Kim, J. H. Yoo, M. Kang, K. Im, R. Grailhe and R. Song, *J. Phys. Chem. C*, 2010, **114**, 21077–21082.
31M. Longmire, P. L. Choyke and H. Kobayashi, *Nanomed.*, 2008, **3**, 703–717.
32W. Yu, W. Xu, H. Song and S. Zhang, *Dalton Trans.*, 2014, **43**, 6139–6147.
33X. Chen, D. Peng and F. Wang, *Nanomaterials*, 2013, **3**, 583–591.
34A. Podhorodecki, M. Banski, A. Noculak, B. Sojka, G. Pawlik and J. Misiewicz, *Nanoscale*, 2013, **5**, 429–436.
35D. Chen and Y. Wang, *Nanoscale*, 2013, **5**, 4621.
36R. D. Shannon, *Acta Crystallogr. Sect. A*, 1976, **32**, 751–767.
37M. Banski, A. Podhorodecki and J. Misiewicz, *Phys. Chem. Chem. Phys.*, 2013, **15**, 19232–19241.
38A. P. Mateusz Banski, *J Mater Chem C*, 2012, **1**, 801–807.
39M. Ito, C. Goutaudier, Y. Guyot, K. Lebbou, T. Fukuda and G. Boulon, *J. Phys. Condens. Matter*, 2004, **16**, 1501.
40L. Tu, X. Liu, F. Wu and H. Zhang, *Chem Soc Rev*, 2015, **44**, 1331–1345.

Nanoscale Accepted Manuscript